APPLICATION OF CRITICAL ANGLE IMAGING TO THE CHARACTERIZATION OF CAST STAINLESS STEELS

B.P. Hildebrand, M.S. Good, A.A. Diaz, and E.R. Green

Pacific Northwest Laboratory
Operated by Battelle Memorial Institute
Battelle Boulevard
Richland, WA 99352

INTRODUCTION

Processes for manufacturing centrifugally cast stainless steel (CCSS) pipe in the U.S. before 1976 resulted in a long, columnar microstructure with grain growth oriented along the direction of heat dissipation. Grains formed from this process attained several centimeters in length. After 1976, the process control was improved and a more equiaxed microstructure, more similar to that found in an isostatic casting, was achieved. The two different grain structures have significantly different ultrasonic properties. Although these microstructures are found in piping, cross sectioning of CCSS piping has also exhibited mixed and layered microstructures [1]. These may be more representative of a larger percentage of the CCSS piping used in the nuclear industry. This paper will focus on the pure columnar and equiaxed microstructures, but future work will extend the technique described in this paper to these other, more complicated, systems.

The large grain structure (either equiaxed or columnar) of cast stainless steel affects propagation of ultrasound by causing severe attenuation, changes in velocity, and scattering of ultrasonic energy. Non-uniformities in the velocity of ultrasound cause refraction and reflection of the sound beam, which can cause the location of defects to be incorrectly reported, specific volumes of material not to be examined, examination at inadequate sensitivity levels, or all three. Coherent reflection and scattering of the sound beam at grain boundaries causes ultrasonic indications which are difficult to distinguish from flaw signals. When this occurs in heavy-wall (approximately 3-inches thick) CCSS piping found in the primary piping of some PWRs, ultrasonic examinations can be confusing, unpredictable, and unreliable.

The ability to classify and, in essence, account for a specific microstructure encountered in these examinations, will aid in partially alleviating the indeterminable nature of these materials. The objective here is to use nondestructive measurements to classify the microstructure of centrifugally cast stainless steel samples. The project was designed to examine the ultrasonic responses (amplitude maps) of

Review of Progress in Quantitative Nondestructive Evaluation, Vol. 11
Edited by D.O. Thompson and D.E. Chimenti, Plenum Press, New York, 1992

equiaxed and columnar grained samples utilizing surface wave ultrasonic inspection techniques over a range of frequencies.

Surface waves excited on a liquid/solid boundary can be used to examine material properties in the near-surface region of the solid. The method described here involves a focused ultrasonic source producing longitudinal waves at an average angle of incidence equal to the so-called "Rayleigh" critical angle (RCA). At this angle, an incident longitudinal wave of wavelength λ_L excites a surface wave on the liquid-solid boundary, extracting a large fraction of the energy from the incident beam. The remaining energy, reflected at an equal but opposite angle is intercepted by a point-like receiver and recorded. Since the critical angle is a sensitive function of Poissons' ratio and the shear velocity of the solid, small material property changes in the solid will produce large changes in the phase and amplitude of the received signal. Because the surface wave penetrates the solid to approximately one shear wavelength, λ_s, and the focused spot on the solid has the approximate area, λ_L^2, the total insonified volume is $\lambda_s\lambda_L^2$. Thus, the material properties in this small region directly affect the amount of reflected energy received. If the source-receiver combination is scanned across the material surface, an image of material property changes within a surface layer of thickness λ_s, with spatial resolution λ_L^2, may be produced.

In this report, we discuss the application of this method to imaging the grain structure, as a function of depth, in cast stainless steel. By lowering the frequency, depth of penetration increases, bringing the influence of deeper regions into the image. Unfortunately, the focused spot size also increases unless the numerical aperture of the source is increased correspondingly.

THEORY

The theory of RCA behavior has been thoroughly explored from several points of view, and will not be reviewed in detail here [2-12]. However, we note that all of the cited references assume plane incident waves, either bounded or unbounded. The problem is stated by assuming a plane longitudinal wave impinging on a flat surface at an incident angle which is varied from perpendicular to grazing. The amplitude of the reflected wave is monitored. Classical theory predicts arrival at two critical angles, defined as those angles for which the refraction of transmitted longitudinal and mode converted shear waves reach 90° within the solid [3]. Typically, for steel, the longitudinal critical angle occurs at 17°, and the shear critical angle at 31°. The monitored reflected amplitude as a function of incident angle remains relatively constant except for small positive going "blips" at the critical angle. Fitch appears to be the first to explicitly explore the Rayleigh critical angle phenomenon and suggest practical applications [13-14], although Rollins is the first to publish in a refereed journal [4]. Both make the observation that at an angle of incidence just beyond the shear critical angle (approximately 1°), the reflected amplitude takes a very sharp and deep dip, sometimes to near zero. Accompanying this sharp reduction in amplitude, the signal undergoes a large phase shift of as much as 360°. The width of the region is very narrow, typically 1° at the half-amplitude points. It is also observed that surface waves are generated at this exact angle of incidence. Assuming conservation of energy, the reflected amplitude dip simply indicates the conversion of the incident energy in the longitudinal wave to surface wave energy.

These observations triggered a flurry of activity in an attempt to provide a theoretical basis for the RCA effect. Two main modifications to the classical theory emerged. Richardson introduced attenuation into the classical Hooke's law via the addition of viscous terms in the stress strain relation [5]. He derived an equation for the reflection coefficient which predicted all observed RCA effects with remarkable accuracy. Working independently Merkulova arrived at the same result [7]. Pitts took a different tack by introducing attenuation directly in the wave numbers, arriving at essentially the same result [9].

A complication to the theory arises when the solid is immersed in a coupling fluid, such as water. Then waves leak back into the fluid from the surface wave. For a plane incident wave, this "leaky" wave is also plane, propagating in a direction parallel to the specularly reflected wave. Thus, interference effects can occur, yielding the so-called beam shift.

As was mentioned previously, Fitch was the first to attempt to exploit the RCA effect as a means for studying the surface properties of materials, since the RCA was very sensitive to material variations such as Poissons' ratio, attenuation, and shear velocity. The first attempt to utilize the RCA effect for imaging of surface properties was published by Hildebrand and Becker, in which changes in surface hardness were mapped by scanning two plane wave transducers set at the nominal RCA for the material [15]. Resolution was, however, limited by the transducer diameter. In an attempt to attain high resolution images, Fitzpatrick and Hildebrand modified the experiment by using a focused source and a point-like receiver as shown in Fig. 1 [16]. Linfoot and Wolf have shown that the wave front at the focus of such a source is plane within the Airy disk of diameter $1.22\lambda_w/NA$, where λ_w is the wavelength in the water coupling medium, and NA is the numerical aperture of the source transducer [17]. Thus, this method allows the plane wave theory to hold, even though a very small surface area is insonified. The regions outside the airy disk are reflected away from the RCA, leaving the central ray bundle uncontaminated by diverging rays. Hence, the point-like receiver intercepts only the energy reflected at the RCA. Furthermore, leaky waves are essentially excluded by this method.

EXPERIMENT

An adjustable goniometric fixture was fabricated, and attached to an x-y scanner. The sample surface was placed in the focal plane of the source and levelled to be parallel to the scan plane. The goniometer was adjusted to attain the RCA by monitoring the output of the point-like receiving transducer. When a null in its response is attained, we are assured of having found the RCA of the small area under the focal spot of the source transducer. The goniometer is then scanned over the desired area and a C-scan image produced. Figure 2 is a test image made of a Y-pattern of flat bottomed holes drilled to within λ_s of the surface of an aluminum block. The holes are 4.75 mm in diameter with edges separated by 3, 4, and 5 mm in the three legs of the Y-pattern. The average residual material under the surface is 0.629 mm. A 5-MHz focused transducer of NA = 1/3 produces an Airy disk of 1.1 mm diameter and a shear wavelength in aluminum of 0.626 mm, which is the approximate depth of the induced Rayleigh wave. Note that the holes are clearly imaged with excellent resolution. In this experiment, the RCA was determined away from any hole, so the reflected signal was very small except over the holes.

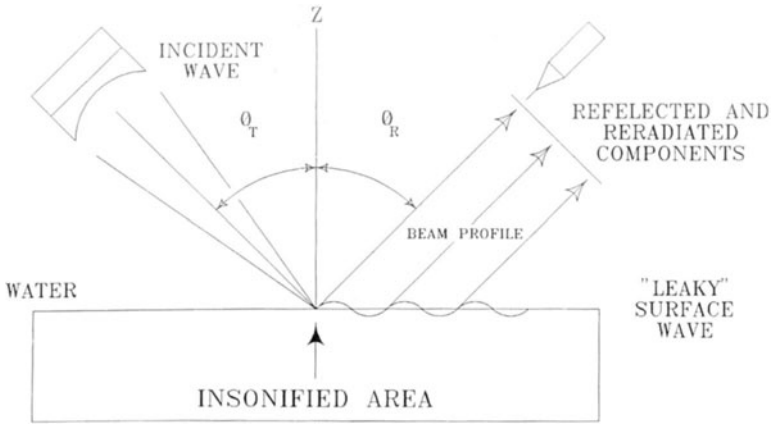

Fig. 1. Geometrical arrangement for RCA imaging.

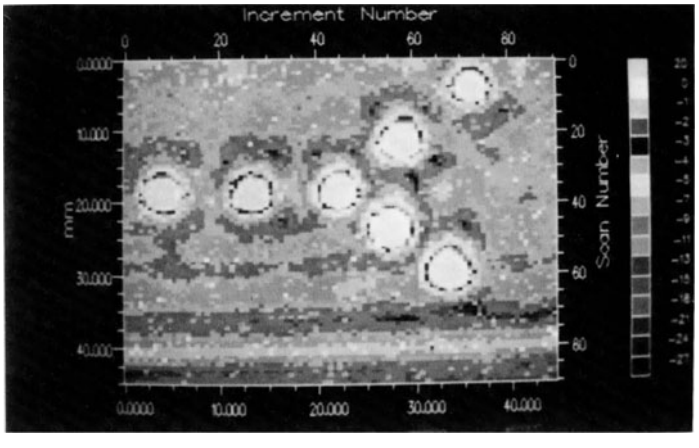

Fig. 2. RCA image of a test pattern of flat-bottomed holes within a shear wavelength of the surface.

The qualitative test shown in Fig. 2 might not satisfy those readers worried about possible leaky wave interference. Consequently, an experiment was devised to prove that only the central ray bundle is measured in this arrangement. The goniometer was once again adjusted to achieve the RCA on a solid block of aluminum. Then the point-like probe was detached from the goniometer and attached to an x-y scanner and scanned over an area somewhat larger than the source transducer.

Figure 3(a) shows this C-scan indicating a "hole" in the center, just where the RCA ray bundle should be. In contrast, Fig. 3(b) shows exactly the same scan when the goniometer is adjusted away from the RCA. There is now only a uniform amplitude across the field. In these photographs, the angle of incidence increases from high to low going from right to left.

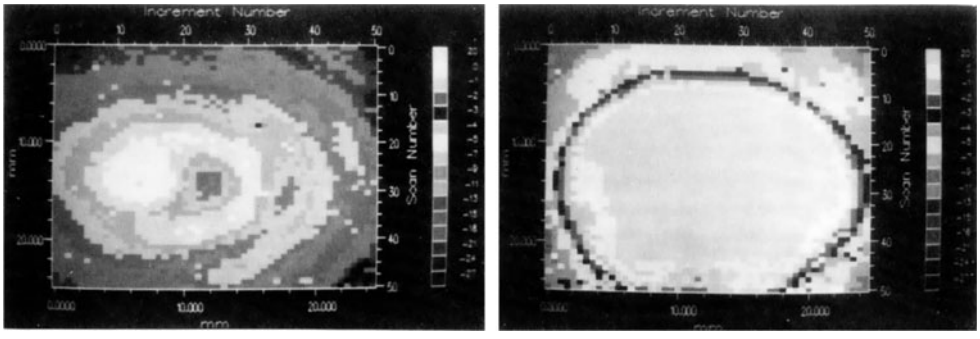

(a) (b)

Fig. 3. Scan of reflected energy when (a) the system is set at the RCA and (b) when it is set at less than the RCA

Figure 4 shows the results of scanning the CSS sample shown in Fig. 4(a) at frequencies of 5, 2.25, and 1 MHz. Note that certain features change as the frequency is decreased, indicating the influence of deeper layers of the sample. Optical features can be correlated with the C-scans by noting that the upper-right corner of Fig. 4(a) corresponds to the upper-left corner in Figs. 4(b), 4(c), and 4(d).

Finally, a number of CCSS pipe samples were scanned at 1, 0.5, and 0.25 MHz using a 0.5-MHz, NA = 0.25 transducer. This means that the depth of the surface layer probed was 3.2, 6.4, and 12.8 mm, respectively. Unfortunately, the size of the focal spot also varies 3.7, 7.4, and 15.8 mm respectively. Thus, images at 250 kHz have much poorer resolution than those at 1 MHz. Figure 5 shows images of the surface of a section of CCSS pipe having a columnar grain structure in the first 12 mm changing to equiaxed below that.

CONCLUSIONS

The RCS imaging technique shows promise as a means for mapping near surface material properties. However, a major problem is that as the frequency is decreased to probe deeper into the material, the spatial resolution decreases as well. Image comparison for different frequencies is therefore compromised. A solution would be a high NA source with a variable aperture to keep the focal spot size constant over the desired frequency range.

ACKNOWLEDGEMENTS

We thank Mr. R. L. Hockey of PNL for spending many hours processing the images.

Work supported by the U.S. Nuclear Regulatory Commission under Contract DE-AC06-76RLO 1830; NRC Program Monitor Dr. J. Muscara; NRC FIN B2289.

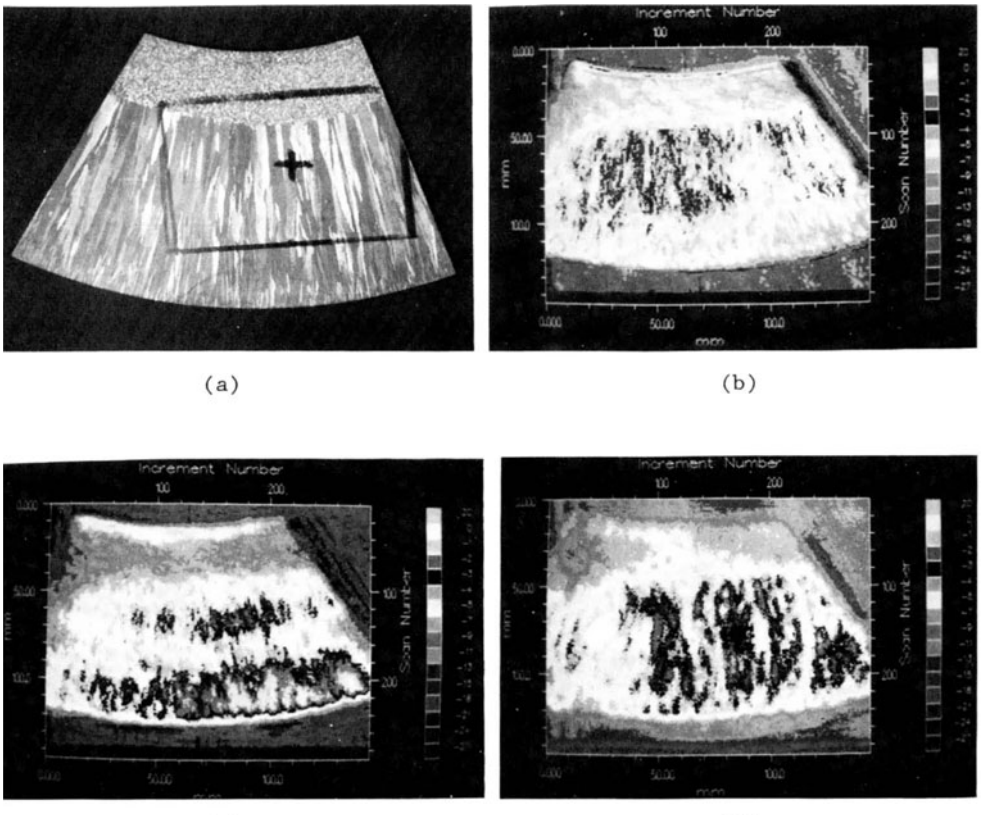

Fig. 4. RCA images at (b) 5 MHz, (c) 2.25 MHz, (d) 1 MHz of the sample shown in (a)

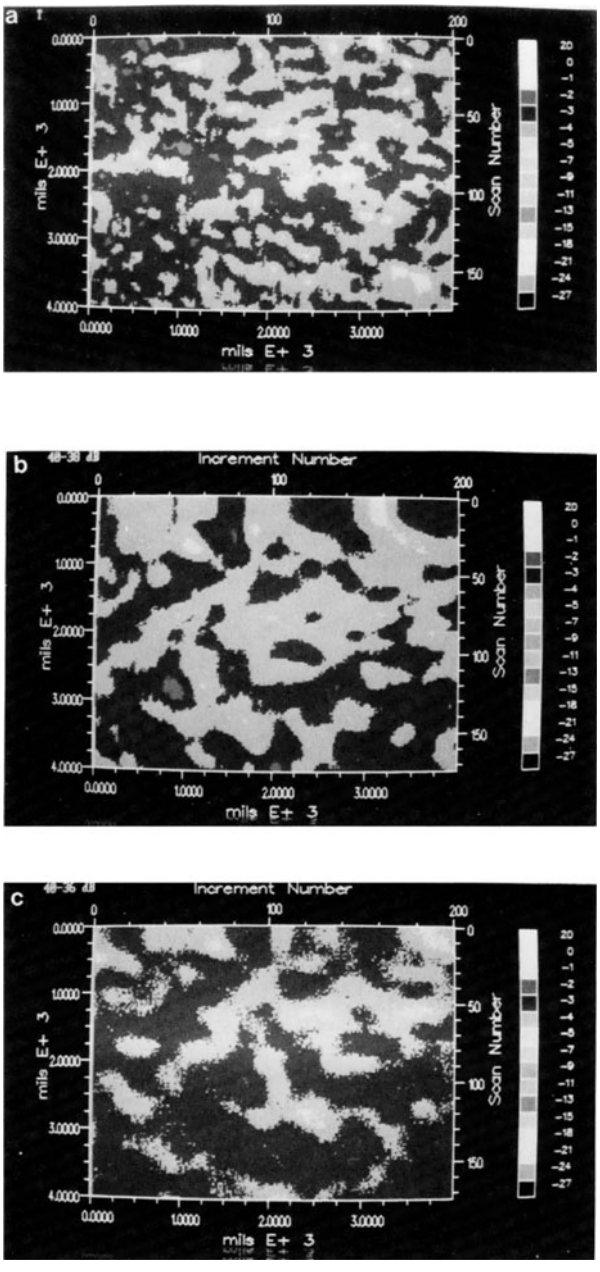

Fig. 5. RCA images at (a) 1 MHz, (b) 500 kHz, and (c) 250 kHz for a CCSS pipe sample

REFERENCES

1. M. S. Good and L. G. Van Fleet, in 8th International Conference on NDE in the Nuclear Industry, edited by D. Stahl (American Society for Metals International, Metals Park, Ohio, 1987), pp. 657-666.
2. A. Schoch, Acustica 2 18 (1952).
3. L. M. Brekhovskikh, Waves in Layered Media (Academic Press, New York, 1960).

4. F. R. Rollins, Jr., Ultrasonic reflectivity at a liquid-solid interface near the angle of incidence for total reflection, Appl. Phys. Lett. 7 (8) (1965).
5. F. L. Becker and R. L. Richardson, J. Acoust. Soc. Am. 51:1609 (1972).
6. F. L. Becker and R. L. Richardson, in Research Techniques in Nondestructive Testing, edited by R. S. Sharpe (Academic Press, London, 1970), pp. 91-130.
7. V. M. Merkulova, Sov. Phys. Acoust. 15:404 (1970).
8. H. L. Bertoni and T. Tamir, Appl. Phys. 2:157-172 (1973).
9. L. E. Pitts, A unified theoretical description of ultrasonics beam reflections from a solid plate in a liquid, Ph.D. Thesis, Georgetown University, Washington, D.C. (1976).
10. L. E. Pitts and T. J. Plona, Theory of nonspecular reflection effects for an ultrasonic beam incident on a solid plate in a liquid, IEEE Trans. Sonics and Ultrasonics, SU-24(2) (1977).
11. T. D. K. Ngoc and W. G. Mayer, J. Acoust. Soc. Am. 67:1149-1152 (1980).
12. I. A. Viktorov, Rayleigh and Lamb Waves, Physical Theory and Applications (Plenum Press, New York, 1967).
13. C. E. Fitch, Jr., Critical angle ultrasonic tests, HW-79928, AEC Research and Development Report (1963).
14. C. E. Fitch, Jr., J. Acoust. Soc. Am. 40(5), 989-997 (1966).
15. B. P. Hildebrand and F. L. Becker, J. Acoust. Soc. Am. 56:459-462 (1974).
16. G. L. Fitzpatrick and B. P. Hildebrand, Journal of Nondestructive Evaluation, 3:201-220 (1982).
17. E. H. Linfoot and E. Wolf, Proc. Phys. Soc. B:827 (1956).